Characterization of the Heme Binding Properties of *Staphylococcus aureus* IsdA†

Christie L. Vermeiren,‡ Mark Pluym,§ John Mack,§ David E. Heinrichs,*,‡ and Martin J. Stillman*,§

Department of Microbiology and Immunology, Schulich School of Medicine and Dentistry, University of Western Ontario, London, Ontario, Canada N6A 5C1, and Department of Chemistry, University of Western Ontario, London, Ontario, Canada N6A 5B7

Received April 20, 2006; Revised Manuscript Received August 29, 2006

ABSTRACT: We report the first characterization of the physical and spectroscopic properties of the *Staphylococcus aureus* heme-binding protein IsdA. In this study, a combination of gel filtration chromatography and analytical centrifugation experiments demonstrate that IsdA, in solution, is a monomer and adopts an extended conformation that would suggest that it has the ability to protrude from the staphylococcal cell wall and interact with the extracellular environment. IsdA efficiently scavenged intracellular heme within *Escherichia coli.* Gel filtration chromatography and electrospray mass spectrometry together showed that rIsdA in solution is a monomer, and each monomer binds a single heme. Magnetic circular dichroism analyses demonstrate that the heme in rIsdA is a five-coordinate high-spin ferric heme molecule, proximally coordinated by a tyrosyl residue in a cavity that restricts access to small ligands. The heme binding is unlike that in a typical heme protein, for example, myoglobin, because we report that no additional axial ligation is possible in the high-spin ferric state of IsdA. However, reduction to ferrous heme is possible which then allows CO to axially ligate to the ferrous iron. Reoxidation forms the ferric heme, which is once again isolated from exogenous ligands. In summary, rIsdA binds a five-coordinate, high-spin ferric heme which is proximally coordinated by tyrosine. Reduction results in formation of five-coordinate, high-spin ferrous heme with a neutral axial ligand, most likely a histidine. Subsequent addition of CO results in a six-coordinate low-spin ferrous heme also with histidine likely bound proximally. Reoxidation returns the tyrosine as the proximal ligand.

Staphylococcus aureus is a notorious Gram-positive human pathogen. This bacterium is the causative agent of a wide array of both hospital- and community-acquired infections that range from superficial wound lesions to more severe infections such as endocarditis, osteomyelitis, and bacteremia (*1*). The success of this organism as a pathogen is indicative of the elaborate means by which it is able to withstand host defenses (*2*, *3*). One important host defense mechanism is to make the acquisition of iron by the pathogen difficult. Essentially all host iron is bound by transport and storage proteins; ferritin and hemoglobin sequester most intracellular iron, while extracellular iron is guarded by the glycoproteins transferrin in serum and lymph and lactoferrin in external secretions (*4*). Many bacterial pathogens, including *S. aureus*, have adopted specialized mechanisms for acquiring this metal from the host (for recent reviews, see refs *5*−*10*).

Recently, a novel locus, *isd* (iron-regulated surface determinant), has been identified in *S. aureus* (*11*). The *isd* locus, present in all sequenced *S. aureus* genomes as well as in several other Gram-positive bacteria, including *Listeria monocytogenes*, *Bacillus halodurans*, and *Bacillus anthracis*, includes eight genes, encoded from three iron-regulated transcriptional units: *isdA*, *isdB*, and *isdCDEFsrtBisdG*. IsdA, IsdB, and IsdC proteins are covalently anchored to the bacterial peptidoglycan by the activity of enzymes called sortases (*11*, *12*), while the remainder of the *isd* locus encodes proteins that include a predicted membrane protein (IsdD), sortase B (SrtB), a lipoprotein (IsdE), an ATP-binding cassette-type permease (IsdF), and a cytoplasmic protein (IsdG). IsdG has been shown to have heme degrading activity (*13*).

Not unlike other characterized Gram-positive bacterial cell surface proteins, IsdA has been demonstrated to interact with more than one host component. Indeed, it has been demonstrated that IsdA provides physiologically relevant adherence to fibrinogen and fibronectin (*14*) and also that IsdA can interact with several other host components such as transferrin (*14*, *15*) and heme (*16*). IsdA has also recently been shown to be involved in adherence to desquamated human nasal epithelial cells and to enhance colonization of the anterior nares of cotton rats (*17*). The IsdA sequence contains a single NEAT[1] domain (*18*), so named because of its presence in proteins expressed from genes in the vicinity of other genes predicted to encode Fe^{3+} transporters. While IsdA

† This work was supported by operating and equipment grants from the Natural Sciences and Engineering Research Council (NSERC) of Canada (to both D.E.H. and M.J.S.) and the Ontario Graduate Scholarship in Science and Technology program (support to C.L.V.).

* To whom correspondence should be addressed. D.E.H.: e-mail, david.heinrichs@schulich.uwo.ca; phone, (519) 661-3984; fax, (519) 661-3499. M.J.S.: e-mail, martin.stillman@uwo.ca; phone, (519) 661-3821; fax, (519) 661-3022.

‡ Department of Microbiology and Immunology, Schulich School of Medicine and Dentistry.

§ Department of Chemistry.

[1] Abbreviations: CD, circular dichroism; MCD, magnetic CD; ESI-MS, electrospray ionization mass spectrometry; NEAT, near iron transporter; rIsdA, recombinant IsdA.

10.1021/bi0607711 CCC: $33.50
Published on Web 10/03/2006

and IsdC each contain one NEAT copy, IsdB possesses two copies while HarA (also called IsdH) contains three copies (*19*). Although NEAT domains have now been identified in a growing number of Gram-positive surface proteins, the exact function of this domain has yet to be determined; however, expressed in recombinant form, IsdA NEAT has fibrinogen binding ability (*14*), while the two most N-terminal HarA (IsdH) NEAT domains, designated D1 and D2, are associated with hemeoglobin−haptoglobin binding (*19*).

Although there is evidence supporting the role of IsdA as a broad-spectrum adhesin, this protein was initially suggested to play a role in iron acquisition given that (i) the *isd* transcripts are iron-regulated, (ii) IsdEF, encoded within the *isd* locus, shares similarity with ABC transporters that transport iron, and (iii) IsdA has the ability to interact with both transferrin and heme (*15*, *16*). The exact role, however, of IsdA in iron acquisition is not clearly understood.

In this study, we have used gel filtration chromatography, analytical ultracentrifugation, ESI-MS, absorption spectroscopy, and MCD spectroscopy to show that rIsdA exists as an extended monomer in solution and that it is bound to a single heme molecule. The native heme−rIsdA complex exists as a five-coordinate, high-spin ferric heme with restricted access to axial anionic ligands. Reduction to ferrous heme allows access to ligands, and significantly, this reaction is reversible so that subsequent reoxidation prevents access.

EXPERIMENTAL PROCEDURES

Cloning, Overexpression, and Purification of Recombinant IsdA. The majority of the *isdA* gene, corresponding to amino acids 49−316 (excludes signal sequence and C-terminal sorting signal), was cloned into the GST fusion vector pGEX-2T-TEV (*20*) to generate pGST-IsdA. Overexpression of GST-tagged IsdA in *Escherichia coli* ER2566 (protease-deficient) was achieved by growing plasmid-containing cultures in Luria-Bertani broth (Difco) at 37 °C to an optical density at 600 nm of approximately 0.8. Isopropyl β-thiogalactopyranoside (IPTG, 0.4 mM) was added, and cultures were grown for a further 20 h at room temperature. Ampicillin (100 μg/mL) was incorporated into all growth media. Bacterial cells were pelleted, resuspended in phosphate-buffered saline (PBS), and lysed in a French pressure cell. Insoluble material was removed by centrifugation at 100000*g* for 20 min. The GST−IsdA fusion protein was purified when the cell lysate was passed across a 20 mL GSTPrep column (Amersham Biosciences). The GST−IsdA protein was eluted from the column with 10 mM reduced glutathione, 100 mM NaCl, and 50 mM Tris-HCl (pH 9.0). Fusions were cleaved overnight at 4 °C with AcTEV protease (Amersham Biosciences) according to the manufacturer's instructions. Cleaved GST was removed by two passages across a GSTPrep column and collection of the flow-through.

Gel Filtration Chromatography. Analytical gel filtration chromatography was carried out using a Superdex 200 10/30 GL column (Amersham) coupled to a FPLC system (Pharmacia). The column was equilibrated with 50 mM phosphate buffer (pH 7.2) and 150 mM NaCl. Sample volumes of 500 μL were injected into the column and eluted at a flow rate of 200 μL/min. Protein was followed by absorption measurements at 280 nm. The column was calibrated with blue dextran (void volume), β-amylase from sweet potato (200 kDa), alcohol dehydrogenase from yeast (150 kDa), bovine serum albumin (66 kDa), carbonic anhydrase from bovine erythrocytes (29 kDa), and cytochrome *c* from horse heart (12.4 kDa).

Analytical Ultracentrifugation. Prior to sedimentation analysis, rIsdA was dialyzed extensively in phosphate-buffered saline, and the dialysis buffer was retained for use in the reference sector for all runs. Analytical ultracentrifugation was carried out in a Beckman XL-A centrifuge with a four-hole An-60Ti rotor. Absorbance measurements were taken at 280 nm at protein concentrations to bring the absorbance readings into the range of 0.1−1.0. Unless otherwise specified, all data analysis was carried out using Beckman Origin 6.03. For sedimentation runs, cells incorporating six-sector Epon charcoal centerpieces were used. Absorbance measurements were taken in 0.002 cm radial steps and averaged over 10 observations. Equilibrium was attained when absorbance scans taken more than 5 h apart were identical. The partial specific volume of rIsdA was calculated to be 0.725 g/mL at 5 °C. The density of the solvent was calculated to be 1.0069 g/mL at 5 °C. Assuming a single species, the molar mass (M) was determined from the nonlinear least-squares best fit at a single speed according to the equation

$$C_r = C_F\left[\left(\frac{\omega^2}{2RT}\right)M(1-\bar{\nu}\rho)(r^2-F^2)\right] \qquad (1)$$

where C_r is the concentration at radius r, C_F is the solute concentration at reference distance F, ω is the angular velocity of the rotor, $\bar{\nu}$ is the partial specific volume of the solute, ρ is the solvent density, R is the gas constant, and T is the temperature in kelvin. Sedimentation velocity analyses were carried out at 5 °C in cells containing double-sector Epon charcoal centerpieces at 55 000 rpm. Absorbance measurements were taken in continuous mode at a step size of 0.003 without averaging. The cell was scanned every 10 min for a total of 300 min. Sedimentation coefficients were calculated using the time derivative (dc/dt) analysis of Stafford (*21*). The peak of the $g^*(s)$ versus s plot was fitted using a Gaussian distribution. The sedimentation coefficient ($s_{20,w}$), frictional coefficients (f), frictional ratios (f/f_0), and diffusion coefficients ($D_{20,w}$) were calculated using the Origin Technical Graphics and Data Analysis software package (Microcal Software, Inc.).

Spectroscopic Techniques. Electrospray mass spectra were recorded on a Micromass LCT, time-of-flight mass spectrometer operating in the positive ion mode. Absorption (Cary 500, Varian Inc.) and MCD [using an SM2 5.5 T superconducting magnet (Oxford Instruments Ltd., Oxford, U.K.) in a J-820 CD spectrometer (Jasco Inc.)] spectral data were recorded for identical solutions immediately following chemical changes at room temperature. Samples were prepared for spectroscopic and mass spectral analysis as follows. For absorption and MCD measurements, solutions with Soret band absorbances of <0.8 were used. Concentrations were determined by the Bradford assay and using an extinction coefficient of 15 900 M^{-1} cm^{-1} at 280 nm. The pyridine hemochrome test was used to determine the concentration of the heme, as described by Eakanunkul et al. (*22*). Ligand studies with native rIsdA were carried out

by first measuring the absorption and MCD spectra of the native rIsdA with absorption at the Soret band of <0.8 in a 1 cm cuvette and then adding aliquots of the ligand at approximately 5×, 10×, and 25× protein concentrations and then a very large excess, as needed to obtain constant absorption and MCD spectra. The solutions were measured over a period of 1−2 h. Only anionic ligands were added to the native rIsdA ferric solutions. Solutions of the native rIsdA were treated with increasing amounts of crystalline sodium hydrosulfite ($Na_2S_2O_4$) as the reducing agent until no further changes in the absorption and MCD spectra were observed. A key characteristic of ferrous hemes is the absorbance band at 432 nm. Gaseous CO was bubbled slowly into the sealed solutions of the reduced rIsdA through a serum cap until no further changes in the spectrum were measured. For mass spectral measurements, stock solutions of native rIsdA were concentrated to 1−2 mM and then eluted on a G-25 size-exclusion column using 20 mM ammonium formate. Colored fractions were collected and infused at flow rates of 15−20 μL/min into the ESI-MS instrument. The masses determined through the deconvolution program have an estimated standard deviation of ±10 in the 30 000 Da range.

Background to the Use of the MCD Technique for Analysis of Heme-Binding Proteins. MCD spectroscopy typically provides information about the ground- and excited-state orbital degeneracies of high-symmetry complexes based on the Faraday A, B, and C terms (*23*). Key to the analysis of MCD spectral data is the fact that the MCD bands lie at the same energy and exhibit approximately the same bandwidth as the absorption bands. Because we need to refer to the spectral components in the Results, we include a brief description of the origins of the spectrum of a typical iron porphyrin, the model for the heme. In metalloporphyrins, there are two major electronic bands and a strong vibronic band arising from $\pi \rightarrow \pi^*$ transitions: in decreasing energy for Soret (or B) near 405 nm, Q_{vib} or β near 500 nm, and Q_{00} or α near 550 nm; these three bands vary considerably in band maximum and relative intensity. These variations are characteristic of the oxidation and spin state of the central iron. Overlaid on the three bands are charge-transfer transitions between the central metal and the ring, which occur in the same spectral region (*23*). Charge-transfer transitions are particularly sensitive to the oxidation and spin state of the central iron, being observed at different but characteristic wavelengths in the visible region for all but the low-spin ferrous iron. Briefly, for the study described here, in the MCD spectrum of heme proteins, we find derivative-shaped Faraday A terms for species with degenerate excited states and nondegenerate ground states; positive A terms (positive lobe to high energy of the crossover energy) are observed. This will be the case for low-spin ferrous hemes. B terms are Gaussian-shaped bands that arise from interactions between all adjacent states and can be both positively and negatively signed. C terms arise from ground-state degeneracy and give rise at room temperatures to Gaussian-shaped bands of either sign. In iron porphyrins, ground-state degeneracy is found for high-spin ferrous and all spin states of the ferric oxidation state. In addition, pseudo-A terms may be seen when two, oppositely signed C terms exist closely in energy. These pseudo-A terms may be of either sign. In the heme proteins, the MCD spectrum of five-coordinate, high-spin ferrous heme provides an example of a Soret band region characterized by a distorted negative pseudo-A term (*23*).

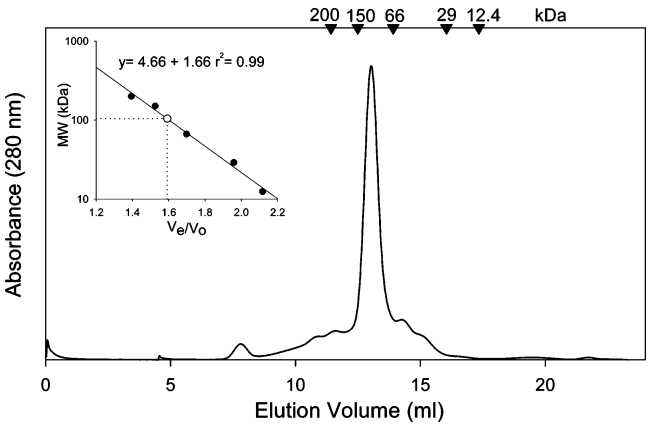

FIGURE 1: Size-exclusion chromatography of IsdA. This chromatogram was obtained from size-exclusion analysis of IsdA using a Superdex 200 column at a flow rate of 0.2 mL/min. The running buffer consisted of 50 mM phosphate buffer and 150 mM NaCl (pH 7.2). The absorbance was recorded at 280 nm. The elution volumes of molecular mass standards are given at the top of the chromatogram. The inset is a calibration curve for the Superdex 200 column. Molecular mass standard proteins were analyzed by size-exclusion chromatography as described above. The elution volume of the standards is represented as a ratio of the elution volume of the protein standard to the void volume of the column (●). The ratio of the elution volume of IsdA is given (○), corresponding to a molecular mass of 100.3 kDa.

Despite this apparent complexity, the MCD spectral bands are diagnostic of the axial ligand identity, spin state, and oxidation state, allowing in many cases unambiguous determination of each of these parameters. This diagnostic sensitivity has been used widely and successfully to interrogate the spin, oxidation, and ligation state of the heme in a wide range of heme proteins (for example, in refs *22*−*27*).

RESULTS

IsdA Is an Extended Monomer in Solution. Heme-containing rIsdA eluted from a size-exclusion chromatography column at a position equivalent to a 100.3 kDa protein (Figure 1). However, the calculated molecular mass of the heme-free rIsdA construct (lacking signal peptide and C-terminal cell wall sorting signal) is 30.06 kDa, while the heme-bound form would be at 30.67 kDa. This result suggested that IsdA either may adopt an extended conformation or may be self-associating. To further investigate these possibilities, the solution properties of the protein were investigated using sedimentation and velocity ultracentrifugation. Sedimentation velocity experiments were performed on rIsdA at initial concentrations between 1.89 and 0.95 mg/mL. The absorbance versus the radial position from the axis of rotation was plotted for each concentration of rIsdA that was used (data not shown) and clearly indicated that IsdA was sedimenting as a monomeric species. The sedimentation coefficient ($s_{20,w}$) calculated for the highest concentration of IsdA tested was 2.4 S, with a calculated frictional ratio (f/f_0) of 1.5, suggesting that IsdA exists as an asymmetric monomer. Assuming a prolate ellipsoidal shape, the axial ratio was calculated to fall between 7 and 10, suggesting that IsdA, in solution, is 7−10 times longer than it is wide. Similar data were obtained for all concentrations of protein

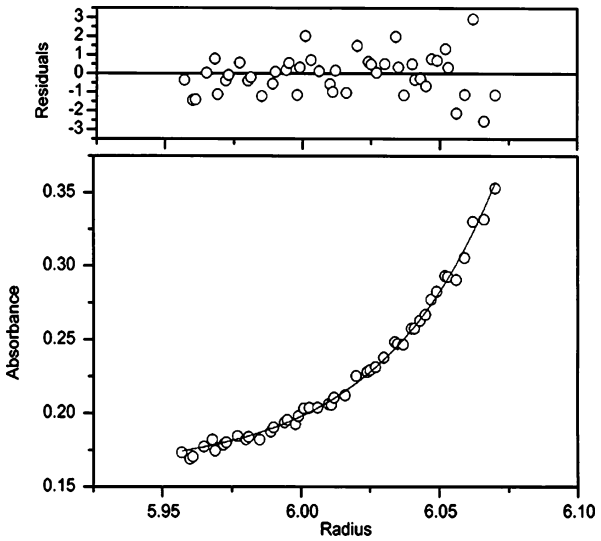

FIGURE 2: Sedimentation equilibrium analysis of IsdA. In the bottom panel, the absorbance at 280 nm is plotted as a function of the radial position. The circles represent the sedimentation equilibrium data obtained for 13 μM IsdA at a rotor speed of 35 000 rpm. The nonlinear least-squares best fit to a single species according to eq 1 is represented by the solid line. The calculated molar mass was 29.4 kDa and is consistent with the molar mass of monomeric recombinant IsdA. In the top panel, the residuals for the nonlinear least-squares best fit are plotted as a function of radial position.

that were tested, demonstrating that the effect is not concentration-dependent. Sedimentation equilibrium experiments were performed on rIsdA under similar solution conditions (Figure 2). The molar mass of rIsdA, at an initial concentration of 13 μM, was calculated using eq 1 to be 29.4 kDa. This is in excellent agreement with the monomeric mass of the expressed heme-free rIsdA (30.0 kDa) or heme-loaded rIsdA (30.67 kDa) and the sedimentation velocity results. Similar results were obtained under these conditions using concentrations of rIsdA between 9 and 26 μM. The mass spectral data (Figure 3) also provided a mass of 30 060 Da for the heme-free rIsdA protein.

Evidence that IsdA Binds Heme in a 1:1 Stoichiometry. When overexpressed and purified from *E. coli*, IsdA is colored, indicating that it is bound to heme. While UV−visible spectroscopy can indicate fine detail of the binding environment of the heme, it is difficult to determine the heme:protein stoichiometry from those spectra. ESI-MS provides detailed stoichiometric and structural information from the mass/charge values, the number of charge states observed, and the subsequent changes in the distribution of these charge states as a function of solution conditions. The charge states arise from protonation of exposed basic residues, generally Lys, Arg, His, and Cys, although protonation of the peptide amide nitrogens is also possible. In addition, monocation and monoanion adducts can displace protons along the peptide chain, resulting in adduct spectra. The exposed residues will be protonated before those residues that are buried in the structure, so if the structure changes as a function of heme binding or denaturation, then the number of residues exposed will change. It is also predicted that denaturation will increase the number of exposed residues and will lead to an increased level of protonation, which in turn will lead to the charge-state distribution being centered on higher numbers. An observation that the center

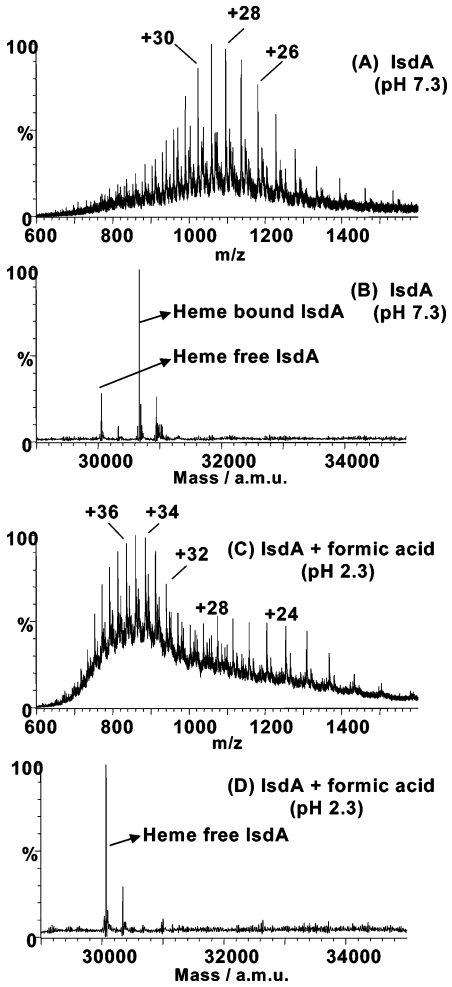

FIGURE 3: Electrospray mass spectra of the expressed IsdA under native and denaturing conditions. (A) At pH 7, the charge states show the presence of conformations centered on the +29 and +31 charged states. (B) The deconvoluted species are assigned as the heme-free protein (mass of 30 055 Da) and the heme-containing protein (mass of 30 671 Da). (C) Electrospray mass spectrum of IsdA following the addition of formic acid, which results in denaturing conditions. The change in the maximum relative abundance indicates a greater degree of protonation compared with that of the native protein. (D) The deconvolution shows that the single species is the heme-free protein with a mass of 30 065 Da.

of the charge-state distribution shifts to higher numbers is strong evidence that the structure has become less folded or more open.

Figure 3A shows the measured charge states for rIsdA at pH 7, with the deconvolution data shown in Figure 3B. The deconvolution shows all unique molecular species that, through protonation, give rise to the large number of measured charge states. These data clearly identify the presence of two predominant molecular species. The major species has a maximum in the charge-state distribution of +29, which corresponds to a mass of 30 671 amu (Figure 3B). This mass arises from protein with one heme bound to one molecule of rIsdA (labeled heme-bound IsdA in Figure 3B). The second species has a maximum intensity near +30 of 30 055 amu, which correlates well with the predicted mass of 30.06 kDa and results from the heme-free rIsdA. We note that the increase of just +1 in the charge-state distribution for the heme-free rIsdA species indicates that only minor structural changes take place in the protein following loss of the heme, compared to changes that take place following

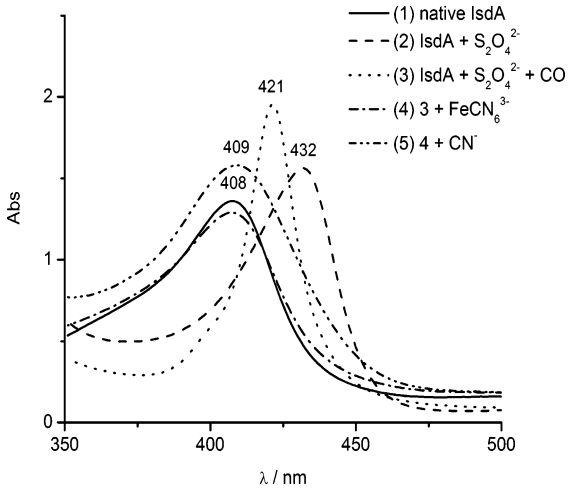

FIGURE 4: Absorption spectra recorded for solutions of rIsdA: (1) native, ferric rIsdA, (2) rIsdA following reduction with sodium hydrosulfite, (3) rIsdA following addition of CO to the reduced rIsdA from trace 2 by bubbling through a serum cap into the sealed cuvette, (4) rIsdA following addition of crystalline potassium ferricyanide to reoxidize the rIsdA solution from trace 3, and (5) rIsdA following addition of cyanide to the reoxidized solution from trace 4.

denaturation (Figure 3C). There is no indication in the ESI mass spectra of a rIsdA species with two bound hemes, which would have a mass of 31 287 amu, and there is also no indication of any other protein species in the solution or of any significant concentration of free heme.

Denaturing rIsdA using formic acid changed the charge-state distribution quite dramatically (Figure 3C). At least two series of charge states are observed, each with the molecular species with a mass of 30 065 amu as the parent molecule (Figure 3D). The predominant series has a charge-state maximum at +35, while the lesser species has maxima between +24 and + 26. Because the parent molecule is the same for both series, this indicates the presence of two or more very different conformations coexisting in solution, one very much more open and, therefore, with more exposed basic residues available for protonation and the other conformation(s) considerably more closed. In both cases, the denaturing conditions resulted in loss of the bound heme. The two minor peaks in Figure 3C are 275 amu higher than the mass of the parent molecule and are present in all the mass spectra. We can account for these peaks as arising from a peptide that is 275 amu heavier due to imperfect cleaving, an impurity that cannot be observed on gels. There is no reason to consider that the additional residues have any effect on the heme binding properties because the heavier peptide appears in each mass spectrum.

The Ferric Heme Iron in rIsdA Is Inaccessible. The optical spectrum of heme-binding proteins is dominated by the absorption bands of the heme between 300 and 700 nm. In particular, the visible region spectrum of the heme in IsdA, which is iron protoporphyrin IX, exhibits a major band near 408 nm (the Soret or B band), followed by a series of bands that extend from 400 to >600 nm, the α/β or Q bands. Figure 4 shows the Soret band absorption spectra of the native rIsdA and the series of liganded species measured as part of this study. The native, ferric rIsdA has a Soret band maximum at 408 nm. No anionic ligands bind to this species. Reduction with sodium hydrosulfite results in the Soret band shifting

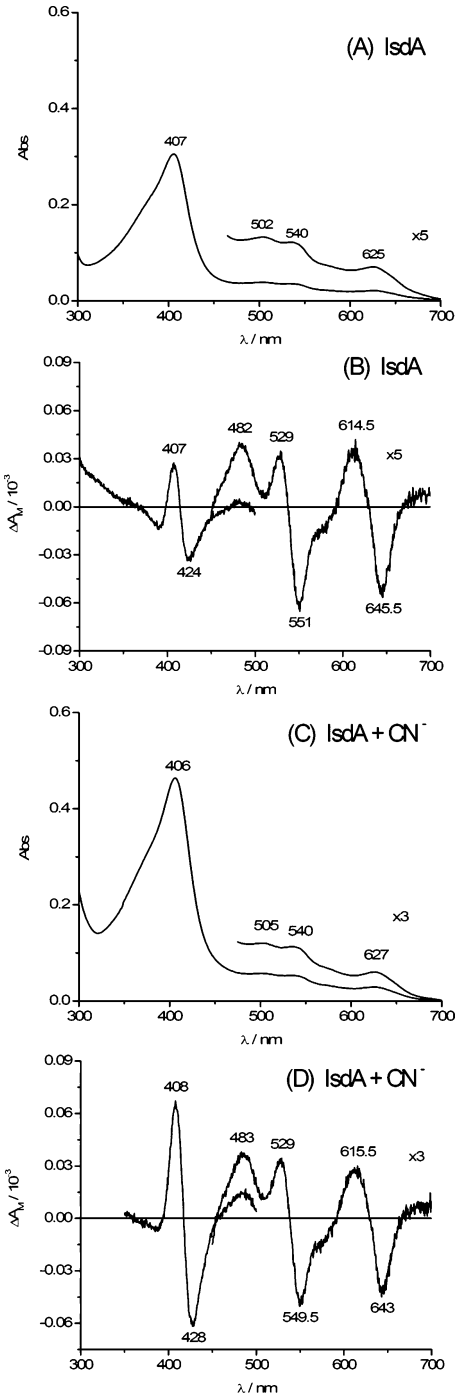

FIGURE 5: Absorption and MCD spectra of ferric IsdA (A and B) as isolated at pH 7 and (C and D) following the addition of crystalline sodium cyanide in small aliquots up to an extremely large excess. No changes were observed in the spectra over a period of hours.

to 432 nm (line 2). Addition of CO to the reduced rIsdA results in a blue shift of the Soret band to 421 nm (line 3). The heme was reoxidized with potassium ferricyanide, resulting in a Soret band shift to 409 nm (line 4), and excess cyanide had no effect (line 5).

In panels A and B of Figure 5, we illustrate the absorption and MCD spectra, respectively, of rIsdA. The band maxima in the absorption spectrum for the Soret band (at 407 nm) and the visible region bands (at 502, 540, and 625 nm) are characteristic of the high-spin ferric heme "fingerprint pattern", which has typically been observed with heme

proteins such as myoglobin with a phenolate axial ligand (*24*). Moreover, the well-characterized absorption and MCD spectra for myoglobin (*25, 26*) provide an excellent model from which to draw conclusions concerning the identity of the fifth and sixth axial ligands of the heme iron in rIsdA since, for myoglobin, spectra have been published for a great many combinations of axial ligand and iron oxidation states (*24*). It is well-established that all the band parameters change as a function of the protein environment of the heme. The spectral changes arise largely as a result of changes that take place at or near the iron, because charge-transfer bands between the metal and the ring overlay the π to π^* bands of the porphyrin ring. These bands change in number, wavelength, and intensity depending on the oxidation state (ferrous, ferric, or ferryl) and spin state (low, intermediate, or high) of the iron, and the axial ligands of the iron control the spin.

In heme proteins, the proximal or fifth position axial ligand may be the nitrogen from His, the sulfur from Cys, or the oxide from Tyr. The distal or sixth position ligand may be (i) other residues in the peptide chain, (ii) water that allows full access for small ligands to the iron, (iii) empty, or (iv) empty but with residues in the vicinity of the heme pocket that block access to the iron. Alternatives (i) and (ii) would result in heme spectra characteristic of six-coordinate iron, whereas alternatives (iii) and (iv) would result in heme spectra characteristic of five-coordinate iron. Our interpretation of the MCD spectral data from native rIsdA (Figure 5A,B) is that the heme contains a five-coordinate, high-spin ferric iron with an anionic oxygen ligand, likely from a proximal Tyr, and that the distal site is empty.

Axial coordination of the ferric heme in proteins with the sixth position accessible (for example, in myoglobin rather than in cytochrome *c*) is possible across the entire range of the spectrochemical series, starting with the very low Δ_{OCT} values of the halides and extending to the strong field ligand cyanide. Ligation by anionic ligands such as cyanide is thermodynamically preferred and takes place with strong binding constants. Strong field ligands such as cyanide systematically force a change from high- or intermediate-spin to low-spin if the existing ligand is a weaker field ligand. However, for rIsdA, we find that there is a negligible effect following addition of excess cyanide on the absorption and MCD spectra (Figure 5C,D). This is extremely unusual and contrasts our expectation based on the spectral properties of myoglobin (and other heme proteins), in which the MCD spectrum of the high-spin ferric heme, which is characterized by the well-resolved, derivative-shaped band centered at ca. 540 nm, is replaced with a strong, low-spin marker band at 570 nm in ferric myoglobin (*25, 26*). The implication of the results presented here for the ferric rIsdA is that, in complete contrast with myoglobin, no sixth position (distal) axial ligation takes place in ferric rIsdA. As would be anticipated, therefore, addition of even large excesses of weaker field ligands within the spectrochemical series, such as fluoride and azide, similarly resulted in no spectral changes (data not shown). This implies that while unoccupied in the native protein the distal site is congested and blocked by other residues, which accounts for the inability of free anionic ligands to bind to the high-spin ferric heme. There is evidence in the literature that Tyr binds to ferric heme proximally in both the ShuT periplasmic protein from *Shigella dysenteriae* (*22*) and bovine liver catalase (*27, 28*). In rIsdA, the oxidized ferric heme exists as the high-spin iron (Figure 5) with characteristic spectral properties of a five-coordinate iron. This means that the ferric heme in rIsdA is inaccessible to even very strong ligands so that the central part of the heme may be considered buried inside the protein structure, effectively blocking axial coordination of the Fe^{3+}.

Reduction of the Iron to +2 Allows Access to the Heme Iron. The iron in heme proteins, even the six-coordinate heme in cytochrome *c*, can usually be reduced with reducing agents such as sodium hydrosulfite ($Na_2S_2O_4$) (*29*). This is also the case for rIsdA: reduction of the heme in rIsdA using sodium hydrosulfite results in large red shifts in the Soret band wavelength and MCD spectral band shape (Figure 6A,B). The absorption band maxima of the Soret band (at 432 m) and of the β and α bands (at 558 nm), observed after the addition of $Na_2S_2O_4$, are consistent with the presence of a five-coordinate, high-spin ferrous heme. A much more significant predictor of the oxidation state, spin state, and coordination environment of the iron is the presence of an inverted pseudo-A term in the Soret region (+ve at 434 nm, −ve at 418 nm) within the MCD spectrum and the collapse of all the visible region bands to the set observed between 540 and 600 nm. This spectral pattern provides the definitive fingerprint pattern evidence for this assignment. Upon reduction, therefore, rIsdA clearly forms a high-spin, five-coordinate ferrous heme, with no coordination in the sixth position, just as observed in myoglobin (*24*). Bubbling CO into a sealed solution of the reduced rIsdA results in the immediate formation of low-spin ferrous heme, which is characterized in the MCD spectrum by two intense positive A terms, centered at 421 and 569 nm (Figure 6C,D). Coordination by O_2 or CO results in the formation of low-spin heme with a MCD spectrum dominated by two positive A terms. The relative intensities and band centers are different for the O_2- and CO-bound hemes, allowing ready identification of the axial ligand. This new pattern is characteristic of a ferrous heme with the sixth position coordinated by CO and the fifth position coordinated by His. While this reactivity is similar to that of myoglobin, it is quite unlike that of cytochrome *c* where the CO cannot break either of the two axially coordinated residues (the Met or the His) (*29*). We speculate that the initial reduction takes place at the edge of the heme that is exposed and not the iron center because the anionic hydrosulfite would not be able to reach the ferric center, followed by electron transfer across the porphyrin resulting in the reduction of the iron to the +2 state. This implies that while the iron is inaccessible to ligands, the heme ring is close to or exposed outside the surface of the protein, allowing reduction from the reducing agent.

The Reduction-Induced Structural Changes in rIsdA Are Reversible. Addition of $[Fe^{III}(CN)_6]^{3-}$ to the reduced rIsdA returns the spectral properties to those observed for the native protein (Figure 5A,B), with the sixth position again inaccessible to strong field ligands such as cyanide (Figure 4). This means that the iron has been reoxidized to the ferric high-spin state and also that the heme iron exhibits electronic spectra characteristic of Tyr proximal coordination. Once again, the spectral data show that even excess cyanide cannot bind to the heme−rIsdA complex, providing evidence that access to the iron is again restricted. The significance of these results is that whereas reduction enables access by CO,

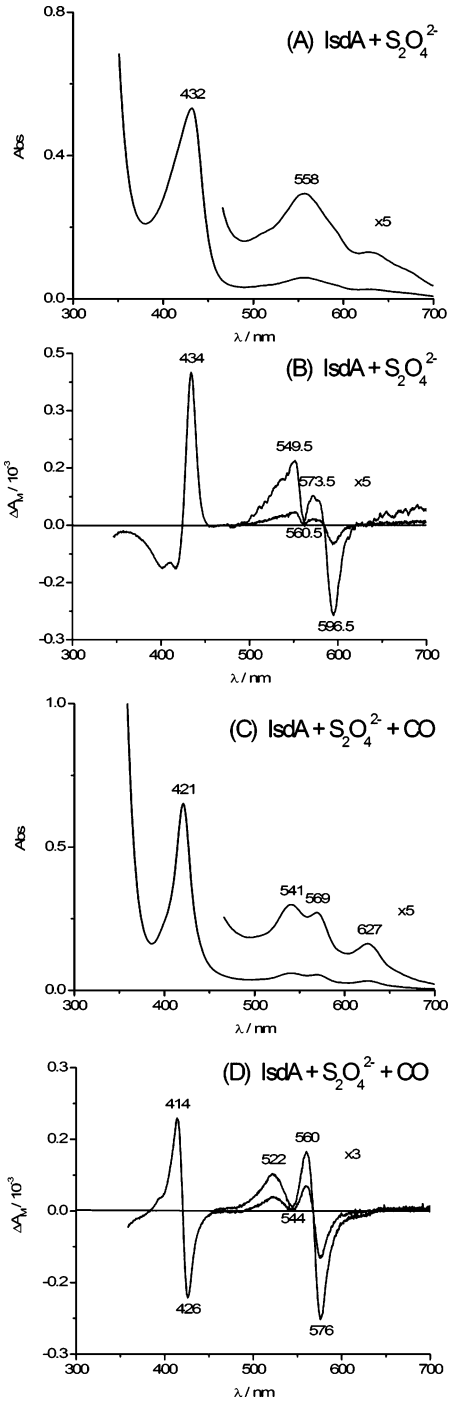

FIGURE 6: (A and B) Absorption and MCD spectra of ferrous IsdA with the addition of sodium hydrosulfite. Crystalline hydrosulfite was added in small aliquots until there were no further changes in the absorption and MCD spectra. The band at 431 nm was monitored and maximized. (C and D) Absorption and MCD spectra of ferrous IsdA with the addition of sodium hydrosulfite and carbon monoxide. CO was bubbled slowly into a sealed solution of reduced rIsdA until no further changes in the intensity of the Soret band at 421 nm were observed.

oxidation restricts this access. The structural model for describing such chemical properties involves a crevice or pocket that reversibly opens following reduction and closes following oxidation of the iron.

DISCUSSION

The iron-regulated surface determinant (*isd*) genetic locus has recently been discovered in the genomes of several different Gram-positive bacterial genera. This genetic locus encodes a series of proteins that have been demonstrated to bind heme and/or heme-containing proteins (*9*, *13*, *16*, *30*). Together, the proteins are thought to represent a novel mechanism for heme acquisition and transport across the Gram-positive bacterial cell envelope. However, to date, the mechanism by which heme proteins are bound by the Isd proteins and the mechanism by which heme itself is bound to the individual proteins and subsequently transferred between proteins are unknown. Biochemical and structural studies of these proteins in the presence of their appropriate ligands are required to establish the role of these proteins in bacterial heme acquisition.

The ESI-MS data in this study clearly demonstrate that rIsdA binds one heme group. The charge-state distributions for the protein with and without the heme are similar, which indicates that there is little rearrangement of the protein secondary or tertiary structures upon heme loss. As expected, CD spectral data (not shown) also show little change between the heme-bound and heme-free protein. Denaturation of rIsdA takes place at low pH with a concomitant large shift in the charge-state maximum from +29 to +35 and loss of heme. It is considered that the more the charge-state distribution shifts toward greater protonation, the more open and more random the protein structure. Following denaturation, we observe two dominant envelopes of bands in the mass spectra shown in Figure 3C; both arise from the same molecular mass (Figure 3D), and neither set includes the heme. The charge states centered on +26 are the same as for the native IsdA in which the heme is bound (except for the slight compensating reduction in mass), whereas the charge states centered on +35 appear only following acidification. We estimate that the relative fraction of the more folded form of the denatured protein is ~30% with a charge-state maximum near +26, whereas 70% adopts the more open structure with the charge states near +35. The +26 set of charge states may arise from the first stage in the unfolding process following loss of the heme. Together, these data correlate well with our analytical ultracentrifugation and gel filtration analyses that indicate that rIsdA adopts an extended conformation in solution.

Not surprisingly, given the relatively recent identification of IsdA, no information existed in the literature describing the environment of the heme bound to IsdA, with the exception of our preliminary report about *E. coli* lysates (*30*). MCD spectroscopy typically provides information about the ground- and excited-state orbital degeneracies of high-symmetry complexes based on positive and negative Gaussian-shaped Faraday B and C terms and the derivative-shaped Faraday A term (*23*). The optical spectra of porphyrinoids are dominated by the intense Soret band in the UV region and by the weaker α and β bands in the visible region, which arise from the B and Q $\pi \rightarrow \pi^*$ transitions of Gouterman's four-orbital model, respectively (*31*). In the case of transition metal porphyrin complexes such as the hemes, there is significant configuration interaction between the B and Q transitions and metal-to-ligand and ligand-to-metal charge-transfer bands.

Changes in the coordination environment of the heme iron, and potential fifth and sixth axial ligation positions above and below the plane of the porphyrinoid ring, result in MCD spectra with substantially modified band morphologies and

sign sequences. Extensive studies of heme binding properties have identified a series of characteristic fingerprint patterns for different heme environments (*24*), which can help to provide answers to a series of questions. (i) How many ligands are attached to the iron in the native state, and what is the nature of these coordinating ligands (nitrogen from His, sulfur from Cys, or oxygen from Tyr, for example)? (ii) Can small axial ligands approach the iron? (iii) Is the heme iron spin state high, intermediate, or low, which relates to the binding strength of the axial ligand present in the native state? (iv) What is the oxidation state of the central iron [Fe(II), Fe(III), or Fe(IV)]?

In the experiments described here, we have taken rIsdA in solution and added, in stepwise fashion, strong-σ donor, anionic axial ligands known to coordinate the heme iron in its ferric state [Fe(III)], which can result in changes in the spin state of the central metal. We have measured the absorption and MCD spectral data for myoglobin with a wide range of anionic axial ligands to compare those data with the rIsdA data presented here (spectral data not shown). Therefore, rIsdA only partially follows the ligation properties observed with myoglobin. No ligation of cyanide takes place with the native ferric protein even in the presence of excess cyanide over periods of hours. These experiments resolve the questions posed above and determine both the electronic structure and the environment of the bound heme.

The MCD spectral data of rIsdA at pH 7 clearly indicate that the ferric iron is coordinated to a weak field ligand, most likely anionic, with Tyr being the key candidate. The MCD data closely resemble those of a number of heme proteins, including catalase in which Tyr is known to be the proximal axial ligand. The lack of cyanide binding indicates that access to the sixth position on the Fe(III) is limited (in this case specifically to anionic ligands) since even in the presence of the excess of cyanide, the distal site could not be reached. Reduction to the ferrous heme, however, allowed access to CO, which suggests that the peptide relaxed in the region of the heme, possibly because the anionic Tyr binds much more weakly to the ferrous iron. This reaction was reversible, and subsequent oxidation back to the Fe(III) again blocked access to cyanide (Figure 4). Reduction of the heme would have to be through an exposed edge of the heme porphyrin as the iron center is not accessible to the anionic hydrosulfite, although the mechanism for the reduction is not clear.

Our conclusions about the environment of the heme in the native rIsdA are that the heme is isolated within the peptide with only an edge accessible, which resembles the situation in cytochrome *c*. The five-coordinate, high-spin ferric iron is inaccessible to anionic axial ligands. Reduction to the ferrous state introduces access to the ferrous iron. The MCD spectral data provide strong evidence that reduction in the absence of exogenous axial ligands leads to the high-spin, five-coordinate ferrous heme in which the proximal ligand is now His. Addition of CO leads to spectral data characteristic of low-spin, six-coordinate ferrous heme, in which the proximal group is also His. These MCD spectral data are almost identical to the well-known data of myoglobin. However, reoxidation again prevents access, providing evidence that the heme has not moved during this chemical process, which suggests that the heme environment is quite stable with respect to chemistry taking place at the heme. In this ferric state, the lack of anionic access, and the band maxima and MCD spectral pattern, again indicate that the proximal group is Tyr. These results suggest that different residues coordinate the heme under these different redox states.

The NEAT domain in IsdA, and included in the rIsdA construct used in this study, contains several Tyr residues that could function in the coordination of the heme molecule. Notably, Tyr87, Tyr102, Tyr166, and Tyr170 are conserved in NEAT domains of IsdA and IsdC which bind heme (*30*, *32*), and also the C-terminal NEAT domains of HarA/IsdH and IsdB from *S. aureus*, and many other NEAT domains identified in the databases. Notably, Pilpa et al. (*32*) have shown that the most N-terminal NEAT domain of IsdH/HarA does not bind heme and lacks these conserved tyrosines, lending support to the idea that at least one of these conserved tyrosines plays an integral role in heme binding. It is interesting to note that of several histidine residues present within IsdA only one, His83, is partially conserved among IsdA, IsdB, IsdC, and IsdH/HarA NEAT domains and may be the residue that provides axial ligation for the heme iron when in the high-spin reduced state, provided that heme is similarly bound by these other NEAT domains. Our ongoing studies will investigate the role of these and other residues in the heme binding ability of the IsdA protein.

ACKNOWLEDGMENT

D.E.H. is a member of the Infectious Diseases Research Group at the University of Western Ontario, and M.J.S. is a member of the Centre for Chemical Physics at the University of Western Ontario. We are grateful to Prof. Stanley Dunn and Ms. Jessica Cai for assistance with analytical centrifugation and acknowledge support from the Canadian Institutes of Health Research for supporting the Biomolecular Interactions and Conformation Facility. We thank Mr. Doug Hairsine for help with the mass spectroscopy.

REFERENCES

1. Tenover, F. C., and Gorwitz, R. J. (2006) in *Gram-positive pathogens* (Fischetti, V. A., Novick, R. P., Ferretti, J. J., Portnoy, D. A., and Rood, J. I., Eds.) pp 526−534, ASM Press, Washington, DC.
2. Novick, R. P. (2006) in *Gram-positive pathogens* (Fischetti, V. A., Novick, R. P., Ferretti, J. J., Portnoy, D. A., and Rood, J. I., Eds.) pp 496−516, ASM Press, Washington, DC.
3. Weiss, J., Bayer, A. S., and Yeaman, M. (2006) in *Gram-positive pathogens* (Fischetti, V. A., Novick, R. P., Ferretti, J. J., Portnoy, D. A., and Rood, J. I., Eds.) pp 544−559, ASM Press, Washington, DC.
4. Bullen, J. J., and Griffiths, E. (1999) *Iron and infection: Molecular, physiological and clinical aspects*, 2nd ed., John Wiley and Sons, New York.
5. Byers, B. R., and Arceneaux, E. L. (1998) in *Iron transport and storage in microorganisms, plants, and animals* (Sigel, A., and Sigel, H., Eds.) pp 37−66, Marcel Dekker,: New York.
6. Genco, C. A., and Dixon, D. W. (2001) Emerging strategies in microbial haem capture, *Mol. Microbiol. 39*, 1−11.
7. Ratledge, C., and Dover, L. G. (2000) Iron metabolism in pathogenic bacteria, *Annu. Rev. Microbiol. 54*, 881−941.
8. Schaible, U. E., and Kaufmann, S. H. (2004) Iron and microbial infection, *Nat. Rev. Microbiol. 2*, 946−953.
9. Skaar, E. P., and Schneewind, O. (2004) Iron-regulated surface determinants (Isd) of *Staphylococcus aureus*: Stealing iron from heme, *Microbes Infect. 6*, 390−397.
10. Wooldridge, K. G., and Williams, P. H. (1993) Iron uptake mechanisms of pathogenic bacteria, *FEMS Microbiol. Rev. 12*, 325−348.
11. Mazmanian, S. K., Ton-That, H., Su, K., and Schneewind, O. (2002) An iron-regulated sortase anchors a class of surface protein

during *Staphylococcus aureus* pathogenesis, *Proc. Natl. Acad. Sci. U.S.A. 99*, 2293−2298.
12. Mazmanian, S. K., Ton-That, H., and Schneewind, O. (2001) Sortase-catalysed anchoring of surface proteins to the cell wall of *Staphylococcus aureus*, *Mol. Microbiol. 40*, 1049−1057.
13. Skaar, E. P., Gaspar, A. H., and Schneewind, O. (2004) IsdG and IsdI, heme-degrading enzymes in the cytoplasm of *Staphylococcus aureus*, *J. Biol. Chem. 279*, 436−443.
14. Clarke, S. R., Wiltshire, M. D., and Foster, S. J. (2004) IsdA of *Staphylococcus aureus* is a broad spectrum, iron-regulated adhesin, *Mol. Microbiol. 51*, 1509−1519.
15. Taylor, J. M., and Heinrichs, D. E. (2002) Transferrin binding in *Staphylococcus aureus*: Involvement of a cell wall anchored protein, *Mol. Microbiol. 43*, 1603−1614.
16. Mazmanian, S. K., Skaar, E. P., Gaspar, A. H., Humayun, M., Gornicki, P., Jelenska, J., Joachmiak, A., Missiakas, D. M., and Schneewind, O. (2003) Passage of heme-iron across the envelope of *Staphylococcus aureus*, *Science 299*, 906−909.
17. Clarke, S. R., Brummell, K. J., Horsburgh, M. J., McDowell, P. W., Mohamad, S. A., Stapleton, M. R., Acevedo, J., Read, R. C., Day, N. P., Peacock, S. J., Mond, J. J., Kokai-Kun, J. F., and Foster, S. J. (2006) Identification of In Vivo-Expressed Antigens of *Staphylococcus aureus* and Their Use in Vaccinations for Protection against Nasal Carriage, *J. Infect. Dis. 193*, 1098−1108.
18. Andrade, M. A., Ciccarelli, F. D., Perez-Iratxeta, C., and Bork, P. (2002) NEAT: A domain duplicated in genes near the components of a putative Fe^{3+} siderophore transporter from Gram-positive pathogenic bacteria, *Genome Biol. 3*, RESEARCH0047.
19. Dryla, A., Gelbmann, D., von Gabain, A., and Nagy, E. (2003) Identification of a novel iron regulated staphylococcal surface protein with haptoglobin-haemoglobin binding activity, *Mol. Microbiol. 49*, 37−53.
20. Sebulsky, M. T., Shilton, B. H., Speziali, C. D., and Heinrichs, D. E. (2003) The role of FhuD2 in iron(III)-hydroxamate transport in *Staphylococcus aureus.* Demonstration that FhuD2 binds iron(III)-hydroxamates but with minimal conformational change and implication of mutations on transport, *J. Biol. Chem. 278*, 49890−49900.
21. Stafford, W. F., III (1992) Boundary analysis in sedimentation transport experiments: A procedure for obtaining sedimentation coefficient distributions using the time derivative of the concentration profile, *Anal. Biochem. 203*, 295−301.
22. Eakanunkul, S., Lukat-Rodgers, G. S., Sumithran, S., Ghosh, A., Rodgers, K. R., Dawson, J. H., and Wilks, A. (2005) Characterization of the periplasmic heme-binding protein ShuT from the heme uptake system of *Shigella dysenteriae*, *Biochemistry 44*, 13179−13191.
23. Mack, J., and Stillman, M. J. (2003) in *The porphyrin handbook* (Kadish, K. M., Smith, K. M., and Guilard, R., Eds.) pp 43−116, Academic Press, New York.
24. Cheek, J., and Dawson, J. H. (2000) in *The handbook of porphyrins and related macrocycles* (Kadish, K. M., Smith, K. M., and Guilard, R., Eds.) pp 339−369, Academic Press, New York.
25. Springall, J., Stillman, M. J., and Thomson, A. J. (1976) Low temperature magnetic circular dichroism spectra of met- and myoglobin derivatives, *Biochim. Biophys. Acta 453*, 494−501.
26. Vickery, L., Nozawa, T., and Sauer, K. (1976) Magnetic circular dichroism studies of myoglobin complexes. Correlations with heme spin state and axial ligation, *J. Am. Chem. Soc. 98*, 343−350.
27. Browett, W. R., and Stillman, M. J. (1979) Magnetic circular dichroism studies of bovine liver catalase, *Biochim. Biophys. Acta 577*, 291−306.
28. Browett, W. R., and Stillman, M. J. (1984) Temperature dependence in the absorption spectra of beef liver catalase, *Biophys. Chem. 19*, 311−320.
29. Schejter, A., Ryan, M. D., Blizzard, E. R., Zhang, C., Margoliash, E., and Feinberg, B. A. (2006) The redox couple of the cytochrome c cyanide complex: The contribution of heme iron ligation to the structural stability, chemical reactivity, and physiological behavior of horse cytochrome c, *Protein Sci. 15*, 234−241.
30. Mack, J., Vermeiren, C., Heinrichs, D. E., and Stillman, M. J. (2004) In vivo heme scavenging by *Staphylococcus aureus* IsdC and IsdE proteins, *Biochem. Biophys. Res. Commun. 320*, 781−788.
31. Gouterman, M. (1979) in *The porphyrins* (Dolphin, D., Ed.) pp 1−100, Academic Press, New York.
32. Pilpa, R. M., Fadeev, E. A., Villareal, V. A., Wong, M. L., Phillips, M., and Clubb, R. T. (2006) Solution structure of the NEAT (NEAr Transporter) domain from IsdH/HarA: The human hemoglobin receptor in *Staphylococcus aureus*, *J. Mol. Biol. 360*, 435−447.

BI0607711